Real-time phase control methods for cold-atom interferometry

Mohamed Guessoum, Nathan Marlière, Charbel Cherfan, Remi Geiger, and Arnaud Landragin*
Laboratoire Temps Espace (LTE), Observatoire de Paris, Université PSL, Sorbonne Université, Université de Lille, National Metrology and Testing Laboratory (LNE), CNRS, 61 avenue de l'Observatoire, 75014 Paris, France

(Received 23 September 2025; revised 25 November 2025; accepted 14 January 2026; published 19 February 2026)

We present two methods to achieve real-time inertial phase compensation in atom interferometers. Both methods, based on jumping of the position of the retroreflection mirror or frequencies of Raman lasers, demonstrate similar state-of-the-art performance on our cold-atom gyroscope, comparable to that of the reference method, based on optical phase jumping. These alternative approaches broaden the scope of applications for real-time inertial phase compensation methods in atomic interferometers, particularly for space applications.

DOI: 10.1103/4fts-8fp8

I. INTRODUCTION

Inertial sensors based on cold-atom interferometry have demonstrated both high sensitivity and accuracy [1] for applications in inertial guidance, geophysics, or the testing of fundamental physics. In most of these sensors, the sensitivity is limited by the sequential nature of the measurements leading to the sampling of acceleration and rotation signals, and by the dead times between measurements. Various methods have been developed to reduce this source of noise and its impact on performance, such as the use of an isolation platform to reduce its contribution [2] and the correlation with conventional sensors to estimate the inertial noise [3]. A further step has been to hybridize the quantum and conventional sensors [4] in order to benefit from their respective advantages of bandwidth and long-term stability. This includes aspects of sensor-data fusion on the one hand and real-time phase compensation (RTC) of vibration noise in the atomic interferometer on the other. In particular, RTC ensures that the interferometer operates at its optimum sensitivity in the middle of its central fringe. The use of these hybridization methods has made it possible to extend the field of application to transportable terrestrial gravimeters [5], on-board gravity measurements [6,7], possibly gravity and acceleration strap-down measurements [8], or acceleration and rotation measurements simultaneously [9,10].

The RTC of the atomic vibration phase alone has been shown to optimize the signal-to-noise ratio of a quantum sensor for gravity measurements [4,5] or acceleration measurements [9], and also for rotation measurements [11,12]. All these sensors are based on the use of two-photon Raman transitions to manipulate atomic wave packets. The method involves applying inertial phase compensation via a phase jump on one of the lasers just before the last recombination pulse. Unfortunately, if we consider atomic sensors in weightlessness, where the two-photon transitions are based on the retroreflection of Raman [13,14] or Bragg [15] lasers, the phase difference between the two lasers no longer plays any role [16]. This is of particular importance for space missions proposed to test fundamental physics [17] or geodesy [18]. This work demonstrates alternative methods to achieve real-time control compatible with space or weightlessness sensors and, more generally, sensors that do not use Doppler shift to lift the degeneracy from opposite Raman or Bragg diffraction processes in retroreflected configuration.

In this paper, we first present our atomic gyroscope setup, then, successively, the two methods based on mirror jumping and frequency jumping, and finally the comparison of the sensitivity to rotation measurement for all the methods. The relevance of these alternative methods is demonstrated by comparing their effectiveness with that of the reference method using phase jumping between Raman laser beams.

II. EXPERIMENTAL SETUP

The experimental setup has been described in previous work [11,19]. Cesium atoms are trapped and cooled inside a three-dimensional magneto-optical trap (MOT) loaded from an adjacent two-dimensional MOT. Using the moving-molasses technique, the atoms are then launched upward, toward the interferometry region, and selected in state $|F = 4, m_F = 0\rangle$. They then undergo an interferometric sequence with a total duration of $2T = 800$ ms comprising four pulses, with area $\pi/2$, π, π, and $\pi/2$, respectively, separated by time intervals $T/2$, T, and $T/2$,

*Contact author: arnaud.landragin@obspm.fr

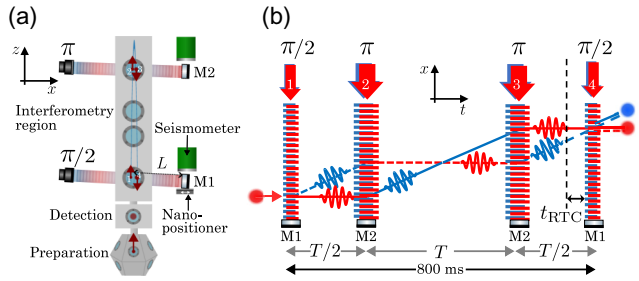

FIG. 1. (a) The scheme of the experimental setup. Atomic clouds are prepared at the bottom of the chamber, launched vertically, and interact with two pairs of Raman lasers in a sequence of four pulses, numbered from 1 to 4, before falling back into the detection area. M1, M2, retroreflection Raman-laser mirrors; L, distance from mirror M1 to the positions of the atom cloud at the fourth pulse. The Raman laser beams are slightly tilted by 4° in the vertical direction. (b) The space-time diagram of the interferometer sequence. Beam splitters and mirrors are realized by a set of Raman pulses of area $\pi/2$ and π. The real-time compensation of the vibrations is applied at a time t_{RTC} just before the beginning of the last beam-splitter pulse. The laser beams at frequency ω_3 (ω_4) are represented in red (blue). The $\pi/2$ pulses (π pulses) are retroflected on mirror M_1 (M_2).

respectively, as sketched in Fig. 1. At the end of the sequence, the phase shift of this state-labeled interferometer is extracted by measuring the transition probability to the state $|F=3, m_F=0\rangle$ by fluorescence means. We apply the phase compensation before the fourth pulse, when the evaluation of the vibration impact can be carried out for almost the entire duration of the interrogation. Nevertheless, a time delay of t_{RTC} is required for it to be fully effective at the time of the last pulse. The phase jump allows for compensation of the inertial phase and then places the measurement point at the midfringe, where the phase sensitivity is maximal.

Atomic beam-splitter ($\pi/2$) and mirror (π) pulses are achieved by using two-photon Raman transitions between the $|F=3\rangle$ and $|F=4\rangle$ hyperfine levels of the ground state. Let us denote the pair of Raman lasers, tuned close to the D_2 line at 852 nm, as L3 and L4. The frequency ω_3 (ω_4) of L3 (L4) is red detuned by Δ to the $|F=3\rangle$-$|F'=3\rangle$ transition (respectively, by Δ to the $|F=4\rangle$-$|F'=3\rangle$ transition). Lasers L3 and L4 are phase locked and have a frequency difference $\delta\omega_L = (\omega_3 - \omega_4)$ in the vicinity of hyperfine splitting, with both the phase and the frequency adjustable in real time. The associated wavelength of laser L3 (L4) is $k_3 = \omega_3/c$ ($k_4 = \omega_4/c$).

In such an interferometer, when the Hamiltonian is at most quadratic in position and momentum, the total phase shift between the two arms can be expressed as a function of the phase difference between the Raman lasers at the center of the atomic wave packets at the pulse times [20]. It can be written in the referential frame of the apparatus as follows:

$$\Delta\Phi = \Phi_{\mathrm{Inert}} + \left[\Phi(0) - 2\Phi\left(\frac{T}{2}\right) + 2\Phi\left(\frac{3T}{2}\right) - \Phi(2T)\right], \tag{1}$$

where Φ_{Inert} is the accumulated phase related to the displacement of the atoms due to inertial forces and $\Phi(t)$ is the difference between the optical phases ϕ_3 and ϕ_4 of the Raman lasers at the positions of the unperturbed trajectory $\mathbf{r}$. This second term in Eq. (1) cancels out in the case of perfect undisturbed Raman lasers.

In practice, we use a configuration in which the two Raman lasers propagate together and are retroreflected on mirrors. We can then apply the so-called k-reversal technique to reduce the contribution of some of the systematic effects [21]. Atoms can then be selectively diffracted in one direction or in the opposite direction, with a transfer of momentum $\pm\hbar\mathbf{k_{eff}}$, where $\mathbf{k_{eff}} = \mathbf{k_3} - \mathbf{k_4}$. To enable this, the direction of the retroreflecting mirrors is slightly tilted by 4° with respect to the horizontal direction in order to lift the degeneracy of resonance conditions due to the opposing Doppler shifts caused by gravity. In this configuration, only one of two retroreflected Raman-laser pairs interacts with the atoms. Moreover, the Raman lasers do not accumulate relative phase noise between the point at which they are locked together and the entrance to the vacuum chamber in which the atoms are manipulated [11]. The phase difference between the two lasers driving the transition is then given by

$$\begin{aligned}\Phi^{\pm}(t) &= \left(\omega_3 t + \phi_3^0 - \mathbf{k}_3^{\pm}\cdot\mathbf{r}\right) - \left(\omega_4 t + \phi_4^0 - \mathbf{k}_4^{\pm}\cdot\mathbf{r}\right)\\ &= \delta\omega_L t + \phi_L \mp \mathbf{k}_{\mathrm{eff}}\cdot\mathbf{r},\end{aligned} \tag{2}$$

where the subscripts $+$ and $-$ indicate the direction of the Raman transition selected to drive the transition, $\phi_L = \phi_3^0 - \phi_4^0$ is the difference in the absolute phase of the two Raman lasers at the entrance to the vacuum chamber, and $\mathbf{r}$ is defined in the referential frame of the instrument.

III. REAL-TIME COMPENSATION METHODS

In our interferometer, the phase due to the difference in laser frequencies cancels out over the four pulses when it is constant (as well as in a three-pulse interferometer case) or linearly ramped. The remaining laser terms to be taken into account for the rest of this paper are as follows:

$$\Phi^{\pm}(t) = \phi_L \mp \mathbf{k}_{\mathrm{eff}}\cdot\mathbf{r}. \tag{3}$$

So far, RTC of the inertial phase by the laser phase has been demonstrated by adjusting the phase difference ϕ_L just before the last pulse [4]. This method compensates Φ_{Inert} from an estimate of classical sensor measurements made during the interrogation. It has been shown to implement the compensation phase well enough to become

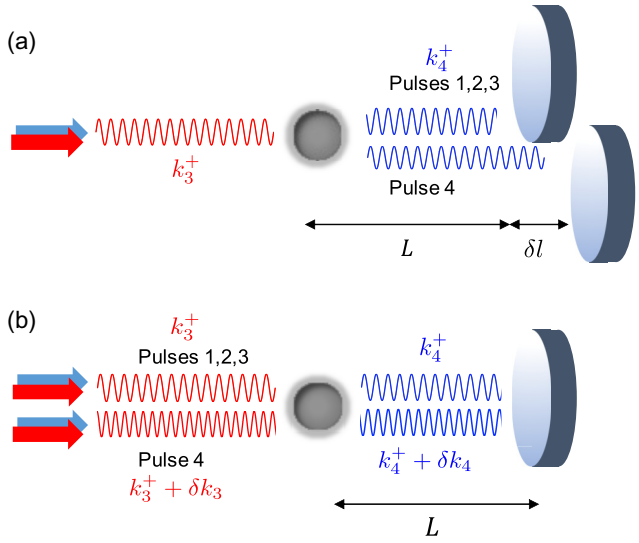

FIG. 2. A schematic diagram of the two alternative methods developed in order to control the output phase of the interferometer. The two Raman lasers are brought together in the experiment and retroreflected on the mirror. Real-time compensation (RTC) is achieved by modifying the optical phase difference between the two counterpropagating Raman light fields at the positions of the atoms before the last pulse: (a) by moving the retroreflecting mirror and (b) by modifying the effective wave vector of the Raman transition. Only the laser fields involved in the transition are shown.

negligible compared to the estimation error itself. It will be used as a reference method to verify the effectiveness of the other two methods and it is detailed in Ref. [19]. However, we can see from the second term of Eq. (3) that two other parameters can be used to change the optical phase and achieve this compensation: the position of the retroreflecting mirror relative to the trajectory of the atom and the modulus of the effective wave vector. These two methods are sketched in Fig. 2 and will be described in detail in the following sections.

A. Mirror-position jumping

The first approach to control the phase of the interferometer consists of changing the position of one of the retroreflecting mirrors. As the first and last pulses (respectively, the second and third pulses) are realized by retroreflection on the same mirror, the absolute distance L to the atoms does not play any role. However, a displacement of δl of the reflective mirror before the last pulse leads to an increment in the total phase shift by

$$\Delta\Phi^{\pm} = \mp k_{\text{eff}}\delta l. \tag{4}$$

Experimentally, this is achieved by mounting retroreflecting mirror M_1 on a voltage-controlled nanopositioner (Mad City Labs model Nano-OP30M). The spanning of one period of the fringes can be done by moving the mirror

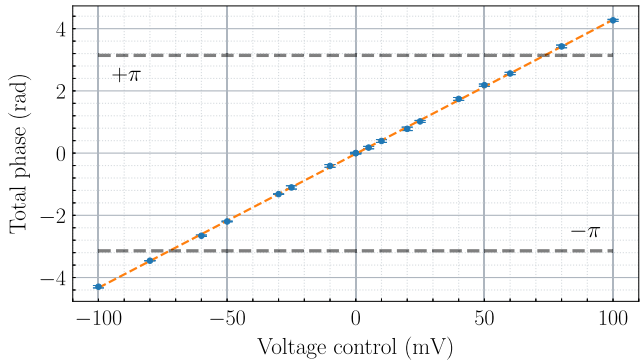

FIG. 3. Variation of the interferometer phase as a function of the mirror displacement between the third and fourth pulses. The x axis shows the control voltage of the nanopositioner. The dots are the experimental results averaged over 700 cycles. The dashed line is the linear fit, with a slope of 43.08(15) rad V^{-1}.

by a distance $\delta l = \lambda/2$, i.e., approximately 426.2 nm. The mechanical displacements follow an almost exponential motion with a time constant of 7.5 ms. Phase compensation is implemented with $t_{\text{RTC}} = 40$ ms, so that the position change is established to better than 99% and t_{RTC} is a multiple of 1/50 Hz (the frequency of the electrical network that causes noise on seismometer signal acquisition). The exact scale factor of the nanopositioner has been determined by integrating measurements of the total interferometer phase while performing constant mirror-position jumping before the last $\pi/2$ pulse for different displacement values (Fig. 3). The characterization results in a scale factor 43.08(15) rad V^{-1} that is constant over the whole range of the applied control voltage. The result corresponds to a displacement of the mirror of 2.92(1) μm V^{-1}, in agreement with the manufacturer's specification of 3.01 μm V^{-1}.

B. Frequency jumping

The second method consists in modifying the effective wave vector of the Raman transition. This is achieved by changing the Raman detuning by a quantity $\delta\Delta$, which means the frequencies of both Raman lasers, $\delta\omega_3 = \delta\omega_4 = \delta\Delta$, while keeping them in phase with each other at a constant frequency difference. When applied before the last pulse, the phase shift added to the interferometer is

$$\Delta\Phi^{\pm} = \mp L\delta k_{\text{eff}} = \mp\delta\Delta\tau, \tag{5}$$

where $\delta k_{\text{eff}} = 2k_{\text{eff}} \cdot \delta\Delta/(\omega_3 + \omega_4)$ is the change of the wave vector and $\tau = 2L/c$ is the delay of retroreflection from the atom to the mirror and back. This sensitivity of the interferometer phase to the change of Raman-laser frequency has been identified and characterized as a potential source of noise [22,23] but also a way of compensating for [24,25] and measuring [26,27] the gradient of gravity. In our experiment, as the distance L is approximately 10 cm, we have needed a frequency jump of about ±800 MHz in

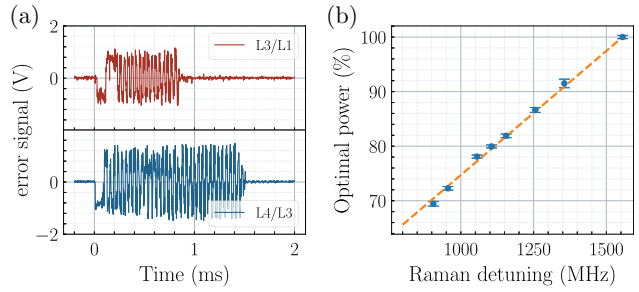

FIG. 4. Characterization of the modifications to the Raman bench in order to achieve a frequency jump while keeping the Rabi frequency constant. (a) The post-frequency-jump time evolution of the error signals from the frequency- and phase-control system of laser L3, at the top, and L4, at the bottom, versus reference locking to lasers L1 and L3, respectively (see text). (b) The relative optimum power to preserve the π- or $\pi/2$-pulse conditions as a function of the Raman detuning. The reference point is set at maximum Raman detuning for $|\Delta| = 1555$ MHz. Each point is deduced from the Rabi oscillations based on measurements over 30 cycles. The dashed orange line is a linear fit of the data points with a slope of 4.6% variation in optimum power per 100 MHz variation of the Raman detuning.

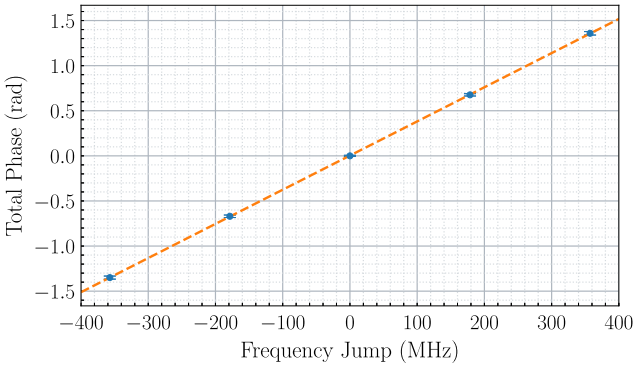

FIG. 5. The atom interferometer phase shift as a function of the frequency jump before the last pulse, while keeping Ω_{Rabi} constant. The dots are the experimental results averaged over 700 cycles. The dashed line represents a linear fit of the experimental data with a slope of 3.786(6) mrad/MHz.

order to achieve a $\pm\pi$ phase shift. However, changing the frequencies of the Raman laser requires further modifications to the laser bench in order, first, to keep both lasers phase locked and, second, to keep the coupling with the atoms, characterized by the Rabi frequency, constant.

The two lasers, L3 and L4, are extended-cavity lasers that can be phase and frequency stabilized by a piezoelectric actuator and a diode current before being optically amplified. Each error signal is generated from a beat note with a master laser, which is compared to a signal controlled by an rf direct digital synthesizer (DDS). Laser L3 is frequency locked with respect to the repumping laser L1, allowing adjustment of the detuning of the Raman transition from $\Delta = -755$ MHz to $\Delta = -1555$ MHz. Laser L4 is then locked to laser L3 and follows it when the latter is modified. The frequency range is chosen around $\Delta = -1155$ MHz, where the dependence of the Raman-laser light shift on detuning is minimal for the cesium atom [21]. The light shift stays below 12% of the Rabi frequency, which allows us to maintain the maximum contrast of the interferometer. To prevent mode hopping during large frequency jumps, a synchronized feedforward mechanism is implemented, simultaneously adjusting both the diode current and the piezoelectric actuator voltage of each laser. Nevertheless, the frequency jump is limited to a range of 800 MHz in total, in order to avoid any unlocking events. Laser L3 (L4) is ready to perform the Raman pulse in less than 1 ms (1.6 ms) [see Fig. 4(a)]. The frequency jump is done with $t_{\text{RTC}} = 20$ ms, so that the frequency change is established and t_{RTC} is a multiple of $1/50$ Hz.

The second modification to the Raman-laser bench is to allow the optical power to be adjusted to compensate for the change in coupling of the Raman transition, i.e., the Rabi frequency, which scales almost as $1/\Delta$, and to preserve the $\pi/2$ and π pulse conditions. This adjustment is carried out on both beams simultaneously, using an acousto-optic modulator that is already in use for pulse shaping. All changes to the Raman lasers associated with frequency jumping during the sequence have been calibrated in advance [for the calibration of the laser-power compensation, see Fig. 4(b)] and fed back into the computer controlling the experiment.

We experimentally determine the scaling factor of this method. Indeed, if the wave vector is very well known, the distance L of the atoms to the reflecting mirror has to be determined by a direct measurement with the interferometer [28]. In Fig. 5, we show the determination of the change of the output phase of the interferometer for a variation of the detuning around $\Delta = -1155$ MHz. The fit leads to an average distance of $L = 90.4(2)$ mm. The value of distance L, combined with the frequency-tuning range of the lasers, enables the interferometer phase to be adjusted over a full range of π. In order to cover the entire range of 2π required for RTC methods, the distance L could be doubled, as could the frequency-jump range, which requires a change in the Raman lasers to prevent unlocking. This full range condition would also be achieved in a double-diffraction configuration, in which the induced atomic phase jump would be twice as large.

IV. PERFORMANCE OF REAL-TIME PHASE COMPENSATION METHODS

The performance comparison of the real-time inertial phase compensation methods is carried out on our gyroscope as described in Ref. [19] but in a continuous-measurement configuration that is not interleaved, as in

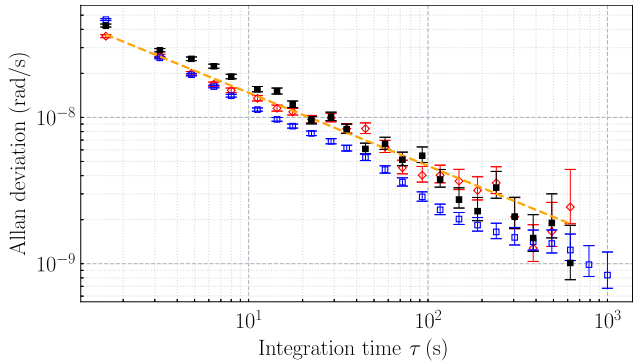

FIG. 6. The standard Allan deviations (ADEVs) of the rotation-measurement stability with different real-time compensation methods: in black, the reference method according to jumping of the difference in the Raman-laser phases; in blue, that according to mirror-position jumping; and in red, that according to combined frequency and phase jumping. The dashed line represents a decay in the $1/\sqrt{\tau}$ characteristic of the white noise.

Ref. [11]. The inertial vibration phase is estimated from broadband seismometers by integrating the impact of the inertial signal weighted by the interferometer sensitivity function [4]. The real-time compensation is applied with a t_{RTC} set at 20 ms for phase and frequency jumping and 40 ms for position jumping. In order to reduce the error due to the absence of signals for the last duration of t_{RTC}, we extrapolate the estimate to the end of the sequence. In practice, we have used the signal recorded during a duration of t_{RTC} before the application of the compensation as a good estimation of the signal after it, as the bandwidth of the seismometer is limited to 50 Hz. In the case of position jumping, the compensation phase is integrated over successive measurements and converted modulo 2π into the mirror position, remaining within a range of $\lambda/2$ around the initial position and avoiding cumulative position errors. In the case of frequency-jump compensation, this is limited to a phase shift of π. This is why only half of the compensation of the inertial phase is applied via a frequency jump, while the remaining half is implemented through a phase jump. In the same way, we have applied the total compensation calculated modulo 2π so that the frequency remains around the initial frequency for $\Delta = -1155$ MHz. The atomic phase signal has been acquired every cycling time, i.e., 800 ms, and has been converted into a rotation-rate measurement using the scaling factor of the gyroscope [29], of 4.62×10^{6} rad s^{-1}/rad.

In Fig. 6, we show a comparison of the Allan standard deviations (ADEVs) of the gyroscope stability with the three RTC methods. Similar forms of behavior are observed for all three methods, with the ADEVs decreasing as $\tau^{-1/2}$, as illustrated by the dashed line. The gain in stability using RTC methods is estimated at a factor of 7 by comparing the ADEV of the estimated vibration phase (unplotted) with that of the interferometer phase measurements after compensation, which confirms the effectiveness of all methods. In addition, the sensitivity of around 5.10^{-8} rad s^{-1} at 1 s is similar to that of the state of the art [19] if we consider that this experiment has not been performed in interleaved mode.

V. DISCUSSION AND CONCLUSIONS

We have demonstrated two methods in order to realize real-time compensation for parasitic vibrations that allows for state-of-the-art performance in our cold-atom gyroscope similar to that of the reference method based on phase jumping between the two Raman lasers.

The first method, based on mirror-position jumping, is the easiest to implement. There are, however, three points to consider. First, the minimum time required for the position change to be complete is about 30 ms, which results in a delay that can prevent an accurate estimation of the vibrational phase. Second, special care must be taken to avoid a systematic error from cumulative position displacements if the mean jump is not zero, due to uncertainty in the knowledge of the nanopositioner scaling factor. In our case, in this preliminary study of the scaling factor with a relative uncertainty of 3×10^{-3}, we can already guarantee that the bias on the rotation measurement corresponds to less than 10^{-9} rad s^{-1}. Third, the method is based on physical displacement, which can lead to synchronous vibrations and possibly to a source of long-term drift or bias. These three points do not represent a limitation in our gyroscope, and can be specifically addressed and reduced in additional studies for each of the applications envisaged.

The second method, based on frequency jumping, has the advantage of using only opto-electronic means, with no moving mechanical parts. The jumps can be almost instantaneous, especially when they are the result of direct frequency synthesis, enabling the compensation phase to be calculated right up to the last moment before the pulse. Furthermore, the optomechanical method for implementing this compensation is the same as for gradient compensation and can therefore be added almost for free. A point of concern is the need to know the distance from the atomic cloud to the retroreflective mirror. As it can be calibrated directly, this is not a limitation in most cases in which this distance is stable over time, but it may need to be addressed specifically for application on board a moving vehicle, in which acceleration will lead to nonlinearity in the compensation process. Finally, this method is slightly more complex, as it requires correction of the Rabi-frequency change by adjusting the laser power. Another improvement would be to independently adjust the power of the two Raman laser beams and not just their sum, in order to ensure compensation for light shift over a wider detuning range.

In conclusion, these two methods are complementary to the reference method based on phase jumping and can be used more generally for both Raman and Bragg diffraction, and in particular when using double-diffraction processes [16,30]. Modifications to the gyroscope are currently being prepared in order to use the double-diffraction method, which will enable the study of the contribution of its new RTC methods in this specific context. Last but not least, the applications for which these methods are most interesting aim to achieve the best performance in the absence of the Doppler effect, as in space equipment [14,17,18], or on the ground for horizontal beam splitters [31], or without the possibility of changing the relative phase between the laser beams.

ACKNOWLEDGMENTS

We acknowledge the financial support from the Centre National d'Etudes Spatiales (CNES), from the Agence Nationale pour la Recherche (project PIMAI, ANR-18-CE47-0002-01), and from a government grant managed by the Agence Nationale de la Recherche under the Plan France 2030 with the reference "ANR-22-PETQ-0005." M.G. acknowledges support from Region Ile-de-France, DIM SIRTEQ. We wish to thank L. Sidorenkov and R. Duverger for their careful reading.

DATA AVAILABILITY

The data that support the findings of this paper are not publicly available. The data are available from the authors upon reasonable request.

[1] R. Geiger, A. Landragin, S. Merlet, and F. Pereira Dos Santos, High-accuracy inertial measurements with cold-atom sensors, AVS Quantum Sci. **2**, 024702 (2020).

[2] J. M. Hensley, A. Peters, and S. Chu, Active low frequency vertical vibration isolation, Rev. Sci. Instrum. **70**, 2735 (1999).

[3] S. Merlet, J. Le Gouët, Q. Bodart, A. Clairon, A. Landragin, F. Pereira Dos Santos, and P. Rouchon, Operating an atom interferometer beyond its linear range, Metrologia **46**, 87 (2009).

[4] J. Lautier, L. Volodimer, T. Hardin, S. Merlet, M. Lours, F. Pereira Dos Santos, and A. Landragin, Hybridizing matter-wave and classical accelerometers, Appl. Phys. Lett. **105**, 144102 (2014).

[5] V. Ménoret, P. Vermeulen, N. Le Moigne, S. Bonvalot, P. Bouyer, A. Landragin, and B. Desruelle, Gravity measurements below $10^{-9}g$ with a transportable absolute quantum gravimeter, Sci. Rep. **8**, 12300 (2018).

[6] Y. Bidel, N. Zahzam, C. Blanchard, A. Bonnin, M. Cadoret, A. Bresson, D. Rouxel, and M. F. Lequentrec-Lalancette, Absolute marine gravimetry with matter-wave interferometry, Nat. Commun. **9**, 627 (2018).

[7] T. E. Jensen, B. Dale, A. Stokholm, R. Forsberg, A. Bresson, N. Zahzam, A. Bonnin, and Y. Bidel, Airborne gravimetry with quantum technology: Observations from Iceland and Greenland, Earth Syst. Sci. Data Discuss. **2024**, 1 (2024).

[8] S. Templier, P. Cheiney, Q. d'Armagnac De Castanet, B. Gouraud, H. Porte, F. Napolitano, P. Bouyer, B. Battelier, and B. Barrett, Tracking the vector acceleration with a hybrid quantum accelerometer triad, Sci. Adv. **8**, eadd3854 (2022).

[9] Q. d'Armagnac De Castanet, C. Des Cognets, R. Arguel, S. Templier, V. Jarlaud, V. Ménoret, B. Desruelle, P. Bouyer, and B. Battelier, Atom interferometry at arbitrary orientations and rotation rates, Nat. Commun. **15**, 6406 (2024).

[10] C. Salducci, Y. Bidel, M. Cadoret, S. Darmon, N. Zahzam, A. Bonnin, S. Schwartz, C. Blanchard, and A. Bresson, Quantum sensing of acceleration and rotation by interfering magnetically launched atoms, Sci. Adv. **10**, eadq4498 (2024).

[11] I. Dutta, D. Savoie, B. Fang, B. Venon, C. L. Garrido Alzar, R. Geiger, and A. Landragin, Continuous cold-atom inertial sensor with 1 nrad/sec rotation stability, Phys. Rev. Lett. **116**, 183003 (2016).

[12] Z.-X. Lu, Z.-W. Yao, H.-H. Chen, Y.-F. Mao, S.-B. Lu, M. Jiang, S.-K. Li, M. Ke, J. Gu, A.-Q. Zhang, R.-B. Li, J. Wang, and M.-S. Zhan, Real-time compensation scheme for the accurate measurement of the differential phase in a dual-atom-interferometer gyroscope, Phys. Rev. A **111**, 033305 (2025).

[13] B. Barrett, L. Antoni-Micollier, L. Chichet, B. Battelier, T. Lévèque, A. Landragin, and P. Bouyer, Dual matter-wave inertial sensors in weightlessness, Nat. Commun. **7**, 13786 (2016).

[14] M. He, *et al.*, The space cold atom interferometer for testing the equivalence principle in the China Space Station, npj Microgravity **9**, 58 (2023).

[15] M. D. Lachmann, *et al.*, Ultracold atom interferometry in space, Nat. Commun. **12**, 1317 (2021).

[16] T. Lévèque, A. Gauguet, F. Michaud, F. Pereira Dos Santos, and A. Landragin, Enhancing the area of a Raman atom interferometer using a versatile double-diffraction technique, Phys. Rev. Lett. **103**, 080405 (2009).

[17] D. N. Aguilera, *et al.*, STE-QUEST—test of the universality of free fall using cold atom interferometry, Class. Quantum Grav. **31**, 115010 (2014).

[18] T. Lévèque, C. Fallet, M. Mandea, R. Biancale, J. M. Lemoine, S. Tardivel, S. Delavault, A. Piquereau, S. Bourgogne, F. Pereira Dos Santos, B. Battelier, and Ph. Bouyer, Gravity field mapping using laser-coupled quantum accelerometers in space, J. Geod. **95**, 15 (2021).

[19] D. Savoie, M. Altorio, B. Fang, L. A. Sidorenkov, R. Geiger, and A. Landragin, Interleaved atom interferometry for high-sensitivity inertial measurements, Sci. Adv. **4**, eaau7948 (2018).

[20] C. J. Bordé, Atomic clocks and inertial sensors, Metrologia **39**, 435 (2002).

[21] D. S. Weiss, B. C. Young, and S. Chu, Precision measurement of $\hbar/m_{\mathrm{Cs}}$ based on photon recoil using laser-cooled atoms and atomic interferometry, Appl. Phys. B **59**, 217 (1994).

[22] J. M. McGuirk, G. T. Foster, J. B. Fixler, M. J. Snadden, and M. A. Kasevich, Sensitive absolute-gravity gradiometry using atom interferometry, Phys. Rev. A **65**, 033608 (2002).
[23] J. Le Gouët, P. Cheinet, J. Kim, D. Holleville, A. Clairon, A. Landragin, and F. Pereira Dos Santos, Influence of lasers propagation delay on the sensitivity of atom interferometers, Eur. Phys. J. D **44**, 419 (2007).
[24] A. Roura, Circumventing Heisenberg's uncertainty principle in atom interferometry tests of the equivalence principle, Phys. Rev. Lett. **118**, 160401 (2017).
[25] G. D'Amico, G. Rosi, S. Zhan, L. Cacciapuoti, M. Fattori, and G. M. Tino, Canceling the gravity gradient phase shift in atom interferometry, Phys. Rev. Lett. **119**, 253201 (2017).
[26] R. Caldani, K. X. Weng, S. Merlet, and F. Pereira Dos Santos, Simultaneous accurate determination of both gravity and its vertical gradient, Phys. Rev. A **99**, 033601 (2019).
[27] C. Janvier, V. Ménoret, B. Desruelle, S. Merlet, A. Landragin, and F. Pereira Dos Santos, Compact differential gravimeter at the quantum projection-noise limit, Phys. Rev. A **105**, 022801 (2022).
[28] G. W. Biedermann, X. Wu, L. Deslauriers, S. Roy, C. Mahadeswaraswamy, and M. A. Kasevich, Testing gravity with cold-atom interferometers, Phys. Rev. A **91**, 033629 (2015).
[29] R. Gautier, M. Guessoum, L. A. Sidorenkov, Q. Bouton, A. Landragin, and R. Geiger, Accurate measurement of the Sagnac effect for matter waves, Sci. Adv. **8**, eabn8009 (2022).
[30] E. Giese, A. Roura, G. Tackmann, E. M. Rasel, and W. P. Schleich, Double Bragg diffraction: A tool for atom optics, Phys. Rev. A **88**, 053608 (2013).
[31] B. Canuel, *et al.*, Exploring gravity with the MIGA large scale atom interferometer, Sci. Rep. **8**, 14064 (2018).